Physiological Organ Motion Prediction and Compensation Based on Multi-rate, Delayed, and Unregistered Measurements in Robot-assisted Surgery and Therapy

Meaghan Bowthorpe and Mahdi Tavakoli

Abstract—Physiological motion makes performing a surgical or therapeutic procedure more difficult for the physician. In heart surgery, the heart is stopped as it is too difficult for the surgeon to follow the heart's beating motion and perform a surgical task. In radiation therapy, respiration causes the cancerous tissue to move, rendering the therapy less effective and possibly damaging to healthy tissue. This paper focuses on controlling a robot, which is used to perform the surgery or therapy, to compensate for the physiological motion along the surgical tool's axis such that the point of interest (POI) on the organ becomes stationary relative to the robot. The difficulty in creating such a system lies in the measurement of the POI's and robot's positions via different sensors that are unregistered, have different measurement rates, and have data acquisition and processing delays. This paper presents Kalman filter based estimation of the organ motion despite the large data acquisition/processing delays and low update rates inherent in some measurements used for robot control in robot-assisted surgeries and therapies. This paper also proposes control systems that compensate for the organ motion despite the delayed, multi-rate and unregistered sensor data allowing the physician to perform a therapeutic or surgical procedure with a teleoperated robot on a seemingly stationary POI.

Nomenclature

C	A controller of a system without a time delay
$\bar{C}$	A controller of a time delayed system
H	Transfer function of a system without a time delay
$\bar{H}$	Transfer function of a time delayed system
R	Input to a controller
Y	Output of a controller
D	Robot-POI distance
P_O	Point of interest position
P_R	Robot position
P_P	Physician position
X	Continuous-time signal
X'	Slowly-sampled discrete-time signal
X''	Fast-sampled discrete-time signal
$\bar{X}'$	Delayed and slowly-sampled discrete-time signal
$\bar{X}''$	Delayed and fast-sampled discrete-time signal
$\hat{X}$	Predicted X'' from $\bar{X}''$ (a discrete-time signal)
${}^R_I T$	Image to robot frame transformation
${}^R X$	A point in the robot frame
${}^I X$	A point in the image frame
EKF	Extended Kalman filter
POI	Point of interest
SP	A Smith predictor

Meaghan Bowthorpe and Mahdi Tavakoli are with the Department of Electrical and Computer Engineering, University of Alberta, AB, Canada. meaghan.bowthorpe@ualberta.ca, mahdi.tavakoli@ualberta.ca

I. Introduction

During surgical or therapeutic interventions, the patient lies still so that the physician can perform a procedure on a specific organ. However, even though the patient is still, the organ may be moving due to physiological motion. This makes the intervention less effective and more difficult to perform. There are two main sources of physiological motion: respiration and heart beat. Two types of interventions that are affected by such physiological motion are radiation therapy treatment of cancerous tissue and surgery on the heart. In radiation therapy treatments, the radiation is aimed towards the target cancerous tissue. If the cancerous tissue is continually moving due to respiration, the dosage will not be concentrated on it and healthy tissue will be treated instead. The second source of physiological motion, heartbeat-induced motion, makes it nearly impossible to operate on a freely beating heart. Other sources of physiological motion, such as hand tremor also make the surgical procedure more difficult for the surgeon to perform. Methods to reduce the effect of the surgeon's hand tremor are discussed in [1], but as this motion does not cause the organ to move, it is outside the scope of this paper.

Currently, different techniques are employed to overcome the aforementioned challenge in radiation therapy. Shirato et al. propose to intermittently run the radiation source such that radiation is emitted only when the point of interest (POI) is not displaced significantly [2]. In other words, when respiratory motion causes the organ and hence, the POI to move away from a fixed location, the radiation source is turned off. Bel et al. automatically reposition the patient couch to cancel the effect of respiration-induced motion in order to keep the POI stationary [3]. This continual motion, however, may be uncomfortable for the patient. If the tissue motion is in-plane with respect to the radiation source, the aperture of the source can be shifted such that its focal point moves in-plane with the tissue [4], [5]. Alternatively, the beam can

be steered in three dimensions electromagnetically, but this poses a challenge in terms of the required equipment cost [6]. CyberKnife has designed a radiation therapy system which automatically repositions the radiation source in near real-time if the POI has moved, but has a very low update rate [7]. The Xsight lung tracking system is an addition to the CyberKnife that tracks lung tumors during respiration without the use of fiducial markers [8]. These methods either increase the length of the procedure, are uncomfortable for the patient, are limited to compensating for the motion in a single direction, are expensive, or have a very low update rate. The robot-assisted motion compensation system presented in this paper will not significantly increase the length of the procedure, will not be uncomfortable for the patient, and can be expanded to compensate for motion in all directions.

Currently, to perform a surgical procedure on the heart, either a mechanical stabilizer is used or the heart is stopped and the patient is connected to a heart-lung machine. A mechanical stabilizer suppresses the heart's beating motion using pressure or suction, but fails to eliminate all of the motion and is only useful for procedures on the heart's exterior surface [9]. Also, a heart-lung bypass increases the patient's risk of stroke and long-term cognitive loss [10], [11]. These are serious side-effects, that could be reduced if the surgeon is able to operate on a freely beating heart. The robot-assisted motion compensation system presented in this paper will cancel the relative motion between the robot and the POI, allowing the physician to operate on a seemingly stationary heart. This will eliminate the risks associated with mechanical stabilizers and heart-lung bypass machines.

II. Robot-assisted Compensation for Physiological Motion

For both of the above categories of interventions, we propose the use of robotic-assistance, which can greatly reduce the difficulties caused by physiological motion. By controlling the robot used by the physician for delivering the therapy or performing the surgery to move in synchrony with the physiological motion in a single dimension, along the surgical tool's axis, the POI can be made motionless with respect to the robot. This will allow for safer and more effective interventions and can lead to the advent of new procedures such as surgery performed on a freely beating heart or radio-therapy on the spine [6], [12]. To this end, first, the POI's position (e.g., the cancerous tissue or the POI on the heart) must be measured in real-time. Computed Tomography (CT) and X-ray images are often used to locate cancerous tissue while endoscopes and ultrasound images are often used to visualize the exterior surface and the interior of the beating heart, respectively. Obtaining these measurements from images creates three main challenges in designing the above-described robot-assisted motion compensating system.

1) *Slowly sampled data from the image sensor*: The POI's motion measurements are taken from images that can be acquired at a rate as low as 20 Hz from an ultrasound scanner or as low as 1 Hz from a CT scanner. If the
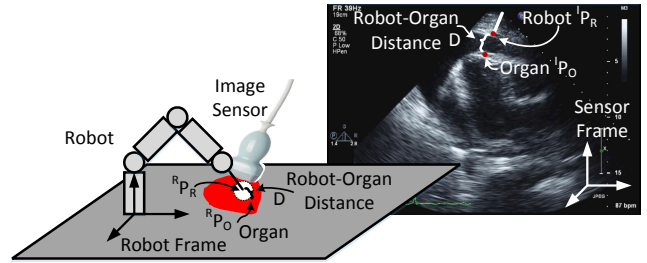

Fig. 1: The robot's position measurements will be recorded with respect to the robot frame and the sensor's position measurements will be recorded with respect to the sensor frame.

robot is controlled to follow these slowly sampled POI position measurements, its motion will not be smooth, which will make performing the procedure not much easier for the physician. Therefore, the slowly sampled position measurements must first be upsampled before being used in the robot's feedback control loop.

2) *Delay in position data acquisition and processing from the image sensor*: To measure the POI's position, an appropriate image-based sensor such as ultrasound scanners, magnetic resonance imaging (MRI) scanners, CT scanners, or endoscopes is used. Depending on the utilized sensor, the data acquisition delay, which is dependent on the sampling rate, may be small as with high-speed endoscopes or large as with ultrasound scanners. Once the image is obtained, it must be processed to locate the POI's position and the robot's position within the image. This processing time varies between image sensors and adds to the acquisition delay. If the delayed position data concerning the POI motion is used in the feedback control loop without delay compensation, the robot control loop may become unstable, possibly leading to uncontrolled collisions between the robot and the POI (in the case of beating heart surgery) or dangerously exposing healthy tissue to radiation (in the case of radiation therapy).

3) *Unregistered frames between data sources*: The POI's position measurements are taken in the image's frame of reference, whereas the robot's real-time position, measured by the robot's encoders, is in the robot's frame of reference - see Fig. 1. If the robot is to follow the POI's motion, the POI's motion must be transformed from the image frame into the robot frame.

Thus, the current POI position must be estimated from the slowly-sampled and delayed image-based measurements of the POI position. Then, a method of repositioning the robot such that it follows the combination of the POI motion and the physician-commanded motion (input through teleoperation) required for the intervention needs to be developed.

Various approaches meeting some of these requirements have been proposed for radiation therapy and beating heart surgery. These techniques can be divided into the following categories based on the type of controller, the position mea-

surements (for position control), and the robot's configuration.

- Robot control: position or force
- POI motion measurement source: images or other sensors
- POI measurements: distances between or positions of organ structures
- POI motion prediction or robot predictive motion control
- Robot configuration: hand-held or teleoperated

Force control can compensate for the POI's physiological motion by maintaining a desired force between the robot and the POI but, it only works when there is contact between the robot and the organ [13]–[15]. Force control does not account for the initial phase of the intervention during which the robot comes into contact with the organ, nor can it be used for certain procedures such as radiation therapy where the robot may never come in contact with the organ. Alternatively, the robot's position can be controlled to follow the combination of the POI's and physician's motions [7], [9], [16]–[22]. Position control is used in this work because of these limitations.

The robot's position can be measured from the robot's encoders in real-time, but measuring the POI's position is more difficult. Different invasive and non-invasive methods of measuring the POI's position have been presented in the literature. In radiation therapy, cancerous tissue is imaged using positron emission tomography (PET), but this exposes the patient to radiation, which is not desirable [23]. For lung biopsies, Xu et al. track a lesion using CT fluoroscopy, which also exposes the patient to radiation [24]. In beating-heart surgery, invasive methods include sonomicrometry crystals, which are sutured to the organ and use ultrasound pulses to determine a single point on the organ's motion [16]–[18]. However, this method only measures the position where sonomicrometry crystals are placed, which is not practical for many interventions as the target site on the organ may change throughout the procedure. Other research uses endoscopes to capture the motion of the organ's exterior surface [9], [19], [25]. These images can be obtained quickly, but cannot visualize the heart's interior due to the opaque blood pool. For this reason, ultrasound images will be used in this research for POI motion tracking in beating-heart surgery [20]–[22].

The difficulty in using images to obtain position measurements is that the positions are measured in the image frame, which is not aligned with the robot's frame. Consequently, the robot cannot be made to follow the POI's position as it is unknown in the robot frame. One possible solution is to have the POI's position measurements transformed into the robot's frame. Then, the robot's position will be controlled to follow the combination of the POI's motion and the physician's motion. The proposed Approach 1 assumes the POI's position measurements can be transformed into the robot frame. If this is not possible, then in the proposed Approach 2, the distance between the robot and POI, which remains the same regardless of the frame of reference, can be measured in the images. The robot-POI distance can then be controlled to follow the physician's motion.

One method of performing the intervention is to attach the aforementioned motion compensating system onto a hand-held tool [20], [26]. In this case, there is no electromechanical dynamic effect between the physician's position and the tool's position. Hand-held robotic surgical tools have previously been developed in [27]. Other systems instead use a teleoperated robot, where the physician's motions are captured by a user interface and then are incorporated into the robot's motion [21]. In this work, a teleoperated robot is considered as it is more intuitive for the surgeon to use than laparoscopic tools, allows the surgeon to sit behind a user console instead of standing at times awkwardly above a patient, offers tools with more dextrous wrists, and allows for a stabilized view of the surgical site to be provided.

Based on the POI motion measurement (POI position or robot-POI distance) and the configuration of the robot chosen (hand-held or teleoperated), different control systems have been presented in the literature. The approaches to compensating for the data acquisition and processing delay can be divided into two methods: prediction algorithms and predictive feedback control. If the robot is hand-held, it will directly follow the physician's motion and the predicted POI's position is fed forward as the reference for the position of the tool attached to the robot. If the robot is teleoperated, predictive feedback controllers, which account for the POI's position measurement time delays in a feedback structure and are thus affected by the dynamic characteristics of the robot, must be used. In both methods the reference position for the robot includes the measurement of the fast-varying heart position. Table I summarizes the above. Approaches 1 and 2 are developed in this paper as discussed later.

The remainder of this paper is organized as follows. The upsampling, prediction, and control systems are described in Sec. III and are tested experimentally in Sec. IV. A functional task where a needle makes contact with a simulated heart is tested experimentally in Sec. V and the results are compared to the literature in Sec. VI. Finally, the concluding remarks are given in Sec. VII.

III. CONTROL SYSTEMS

The choice of the control system depends on the data acquired from the sensors; more specifically, whether or not the position measurements from the images can be transformed into the robot's frame of reference. Regardless of whether the image to robot frame transformation ($^R_I T$) is available, a controller will need to compensate for the image acquisition and processing delay incurred in extracting the slowly sampled position data. If the $^R_I T$ is available, the POI's trajectory is measured directly from the images and transformed into the robot's frame of reference. Then, it is upsampled to the robot trajectory's sampling rate. Next, it is predicted forward from the delayed measurement time to the current time. If the $^R_I T$ is not available, the robot-POI distance is measured in the images and then upsampled. From this distance and the robot's real-time position measurements, the delayed POI's position is calculated and then predicted to the current time. These upsampling and prediction calculations, which are described in detail below, generate the predicted POI motion.

	Control: Position (PC) or Force (FC)	Measurements: Position (P) or Distance (D)	Sensor: Images (I) or Other (O)	Tool: Hand-held (H) or Teleoperated (T)	Control: Prediction (P) or Predictive Feedback (FB)	Control Algorithm
[6]	PC	P	I	T	NA	PID
[9]	PC	P	I	T	P	TT
[12]	PC	P	I	T	NA	AR
[13]	FC	NA	O	T	FB	MPC
[14]	FC	NA	I	T	P	PID
[16]	PC	P	O	T	P	RHMPC +ECG
[17]	PC	P	O	T	P	RHMPC
[18]	PC	P	O	NA	P	MPC
[19]	PC	P	I	T	FB	R-GPC
[20]	PC	P	I	H	P	EKF
[21]	PC	D	I	T	FB	SP
[22]	PC	P	I	T	P	ANN
[28]	PC	P	O	T	FB	MPC
A1	PC	P	I	T	FB	Pro
A2	PC	D	I	T	FB	SP

TABLE I: A summary of the approaches taken to compensate for physiological motion in surgical and therapeutic interventions, where A1 and A2 are the presented approaches 1 and 2 respectively. The following controllers have been presented in the literature: Proportional Integral Derivative (PID), Taken's Theorem (TT), Autoregressive (AR), Model Predictive Control (MPC), Receding Horizon MPC (RHMPC), RHMPC + Electrocardiogram (RHMPC+ECG), Repetitive Generalized Predictive Control (R-GPC), Proportional (Pro), and Artificial Neural Network (ANN).

A. Upsampling of POI Motion Measurements

Many of the sensors such as ultrasound or CT will capture the images at a slower rate than the typical robot control system sampling rate. To take advantage of the robot's faster sampling rate, the slowly sampled position data is upsampled. Two different position measurements may be obtained from the images: the POI's position when the $^R_I T$ is available (Approach 1), or the robot-POI distance when the $^R_I T$ is not available (Approach 2). As the robot-POI distance is to follow the physician's motion, the shape and periodicity of this signal are unknown. On the contrary, the POI's motion will be quasi-periodic as both the heart's beating motion and respiratory motion follow a quasi-periodic trajectory. Accordingly, two upsampling methods are used in this work: cubic interpolation, which does not require a quasi-periodic input signal, and extended Kalman filter (EKF) based upsampling, which does require a quasi-periodic input signal.

To begin, cubic interpolation does not require prior knowledge about the signal and hence, it can be used to upsample either the robot-POI distance or the POI position itself. The following equations describe the upsampled data points $p(i)$.

$$p(i) = h_{00}(i)p_0 + h_{10}(i)m_0 + h_{01}(i)p_1 + h_{11}(i)m_1 \quad (1a)$$
$$h_{00}(i) = 2i^3 - 3i^2 + 1 \quad (1b)$$
$$h_{10}(i) = i^3 - 2i^2 + i \quad (1c)$$
$$h_{01}(i) = -2i^3 + 3i^2 \quad (1d)$$
$$h_{11}(i) = i^3 - i^2 \quad (1e)$$

where p_0 and p_1 are the points in between which the interpolation occurs, m_0 and m_1 are the slopes at points p_0 and p_1, respectively, and i is the interpolation variable and contains evenly spaced values between 0 and 1 and has a length of the number of points, n, to be added between the two slowly sampled points, p_0 and p_1. As four data points are required (points p_0 and p_1 and a data point on either side used to calculate the slope) to ensure that the upsampled signal and its first derivative are continuous, cubic interpolation involves a processing delay of $2n - 1$ sample times.

The second method, upsampling using an EKF, does not increase the data acquisition and processing delay. The input signal has a slow sampling time of ΔT, which is to be increased to a fast sampling time of Δt. However, a model of the input signal is required and hence, the input signal must be quasi-periodic. For this reason, this method can only be used when the $^R_I T$ is available such that the POI motion data can be extracted and fed as the input to the upsampler. First, the EKF is based on the following state space model that evolves through random walk.

$$\mathbf{x}(t + \Delta t) = \mathbf{F}(\Delta t)\mathbf{x}(t) + \mu(t) \quad (2a)$$
$$z(t) = y(\mathbf{x}(t)) + \upsilon(t) \quad (2b)$$

where

$$y(\mathbf{x}(t)) \triangleq c + \sum_{l=1}^{m} r_l \sin \theta_l(t) \quad (3)$$

$$\mathbf{F}(\Delta t) = \begin{bmatrix} \mathbf{I}_{m+1} & \mathbf{0} \\ \mathbf{0} & \begin{matrix} 1 & & & \\ \Delta t & 1 & & \\ 2\Delta t & 0 & 1 & \\ \vdots & & & \ddots \\ m\Delta t & & & & 1 \end{matrix} \end{bmatrix} \quad (4)$$

and $\theta_l(t) = l \int_0^t \omega(\tau)d\tau + \phi_l(t)$, $\mathbf{x}(t) = [c(t), r_l(t), \omega(t), \theta_l(t)]^T$, $\mu(t)$ and $\upsilon(t)$ are independent Gaussian noise terms. In this case, the signal model (3) is based on a Fourier series where the coefficients can vary with time [20], [29]. As this equation is non-linear an EKF is used.

Next, the EKF is updated every time step by the following:

$$\mathbf{P}(t + \Delta t | t) = \mathbf{F}(\Delta t)\mathbf{P}(t|t)\mathbf{F}(\Delta t)^T + \mathbf{Q} \quad (5a)$$
$$S = \sigma_R^2 + \mathbf{H}(\Delta t)\mathbf{P}(t + \Delta t | t)\mathbf{H}(\Delta t)^T \quad (5b)$$
$$\mathbf{K}(t) = \mathbf{P}(t + \Delta t | t)\mathbf{H}(\Delta t)^T S^{-1} \quad (5c)$$

where $\mathbf{P}(t)$ is the estimated covariance matrix, $\mathbf{Q}$ is the process noise covariance matrix, σ_R^2 is the observation noise covariance matrix, and $\mathbf{H}(\Delta t)$ is:

$$\mathbf{H}^T(\Delta t) = \left.\left(\frac{\partial y}{\partial \mathbf{x}}\right)^T\right|_{\hat{\mathbf{x}}(t+\Delta t|t) = \mathbf{F}\hat{\mathbf{x}}(t|t)} \tag{6a}$$

$$= \begin{bmatrix} 1 \\ \sin\hat{\theta}_1(t+\Delta t|t) \\ \vdots \\ \sin\hat{\theta}_m(t+\Delta|t) \\ \hat{r}_1(t+\Delta t|t)\cos\hat{\theta}_1(t+\Delta t|t) \\ \vdots \\ \hat{r}_m(t+\Delta t|t)\cos\hat{\theta}_m(t+\Delta t|t) \end{bmatrix} \tag{6b}$$

where the ˆ symbol denotes the estimated value.

As the EKF upsamples the slowly sampled signal y, with a sampling time of ΔT, a new position measurement $z(t+\Delta t)$ is not available at every time step when the EKF is updated at the fast sample time of Δt. When a new position measurement is available, i.e., Δt is a multiple of ΔT, the estimated covariance matrix $\mathbf{P}$ and the state matrix $\mathbf{x}$ are updated as:

$$\hat{\mathbf{x}}(t+\Delta t|t+\Delta t) = \mathbf{F}(\Delta t)\hat{\mathbf{x}}(t|t) \tag{7a}$$
$$+ \mathbf{K}(t)(z(t+\Delta t) - y(\mathbf{F}(\Delta t)\hat{\mathbf{x}}(t|t))) \tag{7b}$$
$$\mathbf{P}(t+\Delta t|t+\Delta t) = (\mathbf{I} - \mathbf{K}(t)\mathbf{H}(\Delta t))\mathbf{P}(t+\Delta t|t) \tag{7c}$$

When a new position measurement is not available, the estimated covariance matrix $\mathbf{P}$ and the state matrix $\mathbf{x}$ are not updated, but simply propagated ahead one time step as:

$$\hat{\mathbf{x}}(t+\Delta t|t+\Delta t) = \mathbf{F}(\Delta t)\hat{\mathbf{x}}(t|t) \tag{8a}$$
$$\mathbf{P}(t+\Delta t|t+\Delta t) = \mathbf{P}(t+\Delta t|t) \tag{8b}$$

B. POI Motion Prediction

Once the position data has been upsampled, the POI's position is predicted ahead to the current time to overcome the image acquisition and processing delay inherent in image-based POI motion tracking. The POI's motion is either measured from the image directly when the $_I^R T$ is available, or by subtracting the robot-POI distance from the robot's position. Either way, there is a delay in the POI motion tracking. Two methods are used in this work for POI motion prediction and both take advantage of the POI motion's periodicity. The first uses the POI's motion from the last heart beat or respiratory cycle. In this case, the length of the heart beat or respiratory cycle is predetermined and the current POI position is estimated by the corresponding POI position in the previous motion cycle. This method assumes that the respiratory or heart rate does not change. The second is to use an EKF. This method allows the respiratory or heart rate and the amplitude of the motion signal to change. Here, the signal's state matrix $\mathbf{x}$ and the estimated covariance matrix $\mathbf{P}$ are updated every time step as the position signal has previously been upsampled. To predict future points, the state matrix $\mathbf{x}$ is multiplied j times

by the update matrix $\mathbf{F}(\Delta t)$ to move j steps ahead:

$$\hat{\mathbf{x}}(t+j\Delta t|t+\Delta t) = \mathbf{F}(\Delta t)^j\hat{\mathbf{x}}(t+\Delta t|t) \tag{9}$$

C. Robot Predictive Feedback Control

When choosing the feedback control structure, two approaches have been taken in this paper. The first uses position measurements and does not compensate for the delay within the feedback loop, whereas the second uses distance measurements and compensates for the delay within the feedback loop. In both cases, motion compensation is performed along one dimension - the axis of the surgical tool. Let us denote the POI position by P_O, the physician's position by P_P, the robot's position by P_R, and the robot-POI distance by $D = P_R - P_O$. Both continuous signals (e.g., actual POI motion) and discrete-time signals (e.g., measured POI motion) are present within the feedback loop. The continuous time signals are straight lines and the discrete time signals are dotted lines where the distance between the dots is proportional to the sample time, i.e., shorter sample times are shown by dots that are closer together. When referring to a specific variable, say X, let us denote the continuous time signal by X, the slowly-sampled signal by X', the fast-sampled signal by X'', the delayed and slowly-sampled signal by $\bar{X}'$, the delayed and fast-sampled signal by $\bar{X}''$, and the prediction of X'' from $\bar{X}''$ by $\hat{X}$. Also, let us denote a variable measured in the robot frame as $^R X$, and a variable measured in the image frame as $^I X$. Consequently, if the $_I^R T$ is known, the equivalent point in the robot frame can be calculated as $^R X = _I^R T \, ^I X$.

1) Approach 1: In the first approach, the $_I^R T$ is available and both the robot's delayed position, $^I \bar{P}'_R$, and the POI's delayed position, $^I \bar{P}'_O$, are measured in the images. Here, the robot's real-time position, $^R P''_R$, measured from the robot encoders is controlled to follow the combination of the physician's motion, $^R P''_P$, and the estimated POI motion, $^R \hat{P}_O$. As the robot's position, $^R P''_R$, is measured from the robot's encoders and is not delayed, in this case, a regular (non-predictive) feedback controller shown in Fig. 2 is used. Note that, the POI's position, $^I \bar{P}'_O$, is measured with a data acquisition delay in the image frame at the slow sampling rate. This, can be transformed to the robot frame, upsampled to the robot's control rate, and predicted ahead to the current time to obtain $^R \hat{P}_O$. The transfer function of this controller is:

$$^R P''_R = \frac{(^R P''_P + ^R \hat{P}_O)CG}{1+CG} \tag{10}$$

This first method requires the $_I^R T$. However, this transformation may be difficult or infeasible to calculate. For instance, if the position of the sensor (e.g., a hand-held ultrasound probe) changes during the procedure, the $_I^R T$ will need to be recalculated in every sampling time assuming that the ultrasound probe position and orientation can always be tracked. It may become computationally expensive to continually update the $_I^R T$. Also, depending on the configuration of the operating room, measuring the position and orientation of the imaging sensor may be unfeasible.
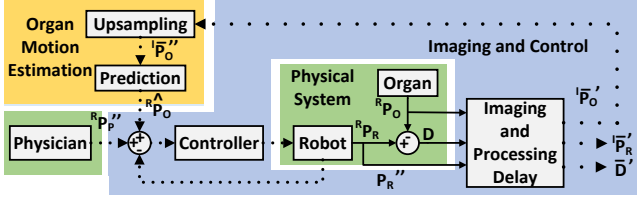
Fig. 2: A simple feedback controller for teleoperated motion compensation. Here, the setpoint for the robot's position, $^{R}P''_{R}$ is the combination of the physician's position, $^{R}P''_{P}$, and the estimated current POI position $^{R}\hat{P}_{O}$.
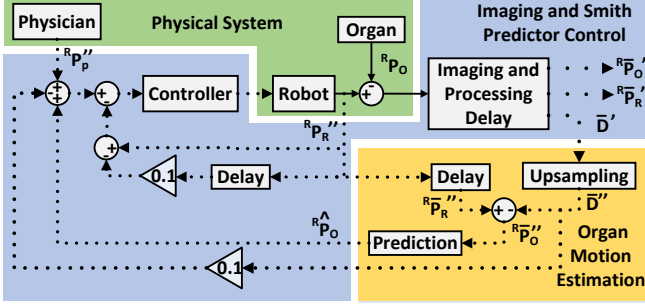

Fig. 3: A SP feedback controller for teleoperated motion compensation when the output is delayed. Here, the setpoint for the robot-POI distance, D, is the combination of the physician's position, $^{R}P''_{P}$, and the estimated current POI position $\hat{P}_{O}$.

2) Approach 2: In cases where the $^{R}_{I}T$ is unavailable, it makes sense to instead rely on the robot-POI distance measured along the surgical tool's axis, D, because this measurement will be the same in any reference frame, i.e. $^{I}D =^{R} D$. This means, the imaging sensor is free to move during the intervention and its position and orientation does not need to be tracked. Note that in this case, either the robot's real-time position, $^{R}P''_{R}$, or the robot's mathematical input-output model (for estimating the position based on the input control signal) must be known. This is because the POI's position, $^{R}\hat{P}''_{O}$ will later need to be calculated based on the robot's position and the measured robot-POI distance. It is important to determine the POI's position as, unlike the robot-POI distance, it is the only quasi-periodic signal available whose current value can be estimated based on delayed measurements using predictive filters.

When the $^{R}_{I}T$ is not available, the robot-POI distance is controlled to follow the physician's motion. The difficulty is that the distance measurement is slowly sampled and delayed, $\bar{D}'$. Cubic interpolation can be used to upsample the signal to $\bar{D}''$, but as the distance signal is not periodic it cannot easily be predicted forward to overcome the delay. Hence, the delay must be compensated for by the controller. In this configuration, the POI's motion acts as a disturbance. Because it is periodic, the POI motion can be predicted and added to the feedback loop. First, the POI's delayed position can be found by delaying the robot's position and subtracting it from the
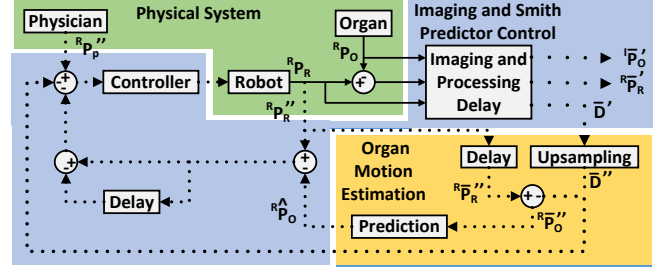

Fig. 4: A SP feedback controller for teleoperated motion compensation with a delayed output. Here, the setpoint for the robot-POI distance, D, is the physician's position, $^{R}P''_{P}$. The estimated current POI position $\hat{P}_{O}$ is added into the inner feedback loop to cancel the effect of the disturbance caused by the POI's motion.

upsampled distance measurement, $^{R}\hat{P}''_{O} =^{R} \bar{P}''_{R} - \bar{D}''$. Now, both the robot's position P''_{R} and an estimate of the delayed POI's position $\bar{P}''_{O}$ are known. With this data, a Smith predictor (SP) is used in the feedback control loop to effectively remove the time delay from within the feedback loop [21], [30]. The Appendix gives a detailed description of the development of the SP.

Two different configurations of the SP, shown in Figs. 3 and 4 are tested. In both cases, the POI's current motion, P_{O}, affects the loop as an external disturbance. To cancel the effect of this disturbance, the predicted POI position, $^{R}\hat{P}''_{O}$, is incorporated into the control system. The point at which the estimated POI position is added into the control loop is the main difference between the two SP configurations. In the first case, it is added to the surgeon's position to form a new setpoint – see Fig. 3. In the second case, it is added to the inner feedback loop to mimic where the disturbance is added to the robot's motion to create the estimated real-time distance signal – see Fig. 4. The possible upsampling and prediction methods for each approach are listed in Table II.

To calculate the transfer function of the first SP configuration, an expression for $\bar{D}'$ is found.

$$(P''_{P} - \bar{D}'' - ((P''_{R} - \hat{P}_{O}) - P''_{R}z^{-k})CG - P_{O})z^{-k} = \bar{D}' \quad (11)$$

where z^{-k} represents the time delay, C is the controller, and G is the robot. Assuming $(P''_{R} - \hat{P}_{O}) = D''$ (11) simplifies to

$$((P''_{P} - \bar{D}'' + P''_{P}z^{-k}CG) - P_{O})z^{-k} = \bar{D}' \quad (12)$$

In this case, $\bar{D}''$ is approximated by $P''_{R}z^{-k}$, which is not ideal. Assuming $D''z^{-k}$ is equivalent to $\bar{D}'$ (12) can be written as:

$$\bar{D}' = \frac{P''_{P}CG - P_{O}}{1 + CG}z^{-k} \quad (13)$$

To calculate the transfer function of the second SP configuration, an expression for $\bar{D}'$ is found.

$$(P''_{P} - \bar{D}'' - ((P''_{R} - \hat{P}_{O}) - (P''_{R} - \hat{P}_{O})z^{-k})CG - P_{O})z^{-k} = \bar{D}' \quad (14)$$

Assuming $(P''_{R} - \hat{P}_{O})z^{-k} = \bar{D}''$ and $P''_{R} - \hat{P}_{O} = D''$ (14)

	Upsampling Method	Prediction Method
Approach 1	CI or EKF	PM or EKF
Approach 2	CI	PM or EKF

TABLE II: The possible upsampling and prediction methods for each approach. CI: cubic interpolation, EKF: extended Kalman filter based upsampling or prediction, PM: previous motion.
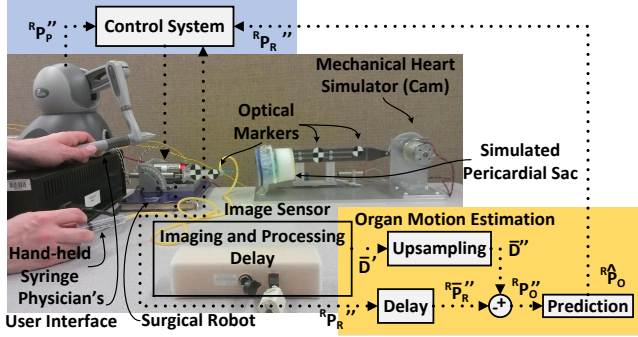

Fig. 6: The simulated heart motion.

Fig. 5: The experimental setup, which includes a mechanical cam that emulates the POI's motion, the image sensor and its optical markers, the physician's user interface, the surgical tool attached to the robot, and the hand-held syringe used for the functional task.

simplifies to

$$((P_P'' - D''CG) - P_O)z^{-k} = \bar{D}' \tag{15}$$

Assuming $D''z^{-k}$ is equivalent to $\bar{D}'$ (15) can be written as:

$$\bar{D}' = \frac{P_P''CG - P_O}{1 + CG}z^{-k} \tag{16}$$

IV. EXPERIMENTAL RESULTS

Each of the controllers, prediction, and upsampling methods were tested experimentally. A Micron Tracker (HX60 from Claron Technology Inc., Toronto, ON, Canada) was used as the image sensor. It has a low frame rate of 20 Hz and a delay of approximately 105 ms in acquiring and storing each frame. A custom-built mechanical cam generated the POI motion. The motion trajectory was collected from the movement of a point on the side wall of the heart in a series of clinical ultrasound images of a patient's beating heart. A single degree-of-freedom (DOF) robot was used and is actuated by a voice coil motor (NCC20-18-020-1X from H2W Technologies Inc., Santa Clarita, CA, USA). To verify the results, real-time position measurements of both the POI and the robot were collected from two potentiometers (LP-75FP-5K and LP-30FP-1K from Midori America Corp., Fullerton, CA, USA): the POI's real-time position is used for robot-POI tracking error calculations only and was not used as a measurement available to the controllers.

For each trial, a cyclic motion with a peak-to-peak amplitude of 10 mm and a period of 63 bpm (0.81 Hz) which is increased to 66 bpm (1.10 Hz) at $t = 10s$ is used. This motion is similar to that encountered when a surgeon punctures the peri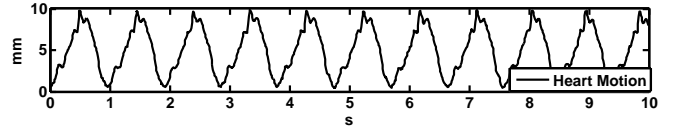cardial sac to drain the excess fluid. Here, the surgeon must puncture the pericardial sac that is approximately 5-10 mm from the exterior heart wall, keep the needle in the pericardial sac long enough to insert a guide-wire without puncturing a coronary artery on the heart wall. This procedure is described further in the following section. Three error metrics are calculated for each trial: the mean absolute error (MAE) between the upsampled and fast discrete-time signal (measured from the potentiometers) is $\frac{\sum |error|}{j}$, where j is the number of data points in the sample, the integral squared error (ISE) is $\frac{\sum (error)^2}{j}$, and the peak error is the largest error at a single point in time. The results from each of the trials are summarized in Table III.

The same parameters were used for the EKF and upsampling in each trial. To find the initial state $\mathbf{x}(0)$ spectral analysis was performed on the mechanical cam's motion. The amplitude, frequency, and number of harmonics were calculated from the Fourier transformation of the mechanical cam's motion. The estimated covariance matrix, $\mathbf{P}(0)$ is initialized to a diagonal matrix with the following values along the diagonal $[0.001, 0.1_{1\times m}, 0.1, 0.2_{1\times m}]$ where m is the number of harmonics, the process noise covariance matrix $\mathbf{Q}$ is a diagonal matrix with a value of 0.0001, and the observation noise covariance matrix σ_R^2 is 0.01. The Micron Tracker supplied image measurements at a rate of 20 Hz or every 50 ms. The robot measurements were collected at a rate of 100 Hz or every 10 ms. To control the robot at the faster rate, four measurements were added via upsampling between measurements of the slowly sampled position signals.

In this work, the following hypotheses are tested.

Hypothesis 1: Predicting and upsampling the POI's motion using an EKF will perform better than using the POI's motion in the last cycle or upsampling using cubic interpolation, because the EKF can adapt to changes in the motion's period and amplitude.

Hypothesis 2: For the case when the $_I^R T$ is not available, the second SP will perform better than the first as the disturbance created by the POI motion is compensated for by the second SP.

A. Approach 1

To begin, the simplest case, where the $_I^R T$ is available, is tested. A simple proportional controller with a gain of 0.2 is used – Fig. 2. The result of each combination of prediction and upsampling method are given in Fig. 7. It can be seen from Fig. 7a and b that using the previous POI positions to predict future POI positions does not take cyclic rate changes into account as the error increases when the heart rate is increased. In this case, the MAE is 1.23 mm, the ISE is 2.39 mm^2,
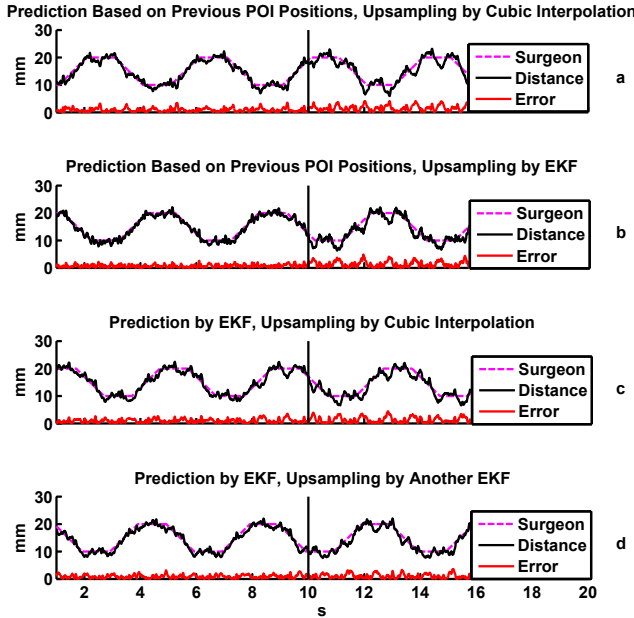
Fig. 7: The tracking result of using proportional control when the $_I^R T$ is available. The dashed pink line is the physician's motion, the solid black line is the real-time distance between the surgical tool tip and the POI, and the solid red line is the error between the surgeon's motion and the real-time robot-POI distance. The vertical line denotes the time at which the heart rate increases.

and the peak error is 4.34 mm when cubic interpolation is used for upsampling in Fig. 7a. The MAE is 1.07 mm, the ISE is 1.99 mm^2, and the peak error is 5.44 mm when EKF based upsampling is used in Fig. 7b. When an EKF is used for prediction in Fig. 7c and d, the cyclic rate change does not affect the error, which remains similar throughout the trial. The MAE is 1.14 mm, the ISE is 2.13 mm^2, and the peak error is 4.38 mm when cubic interpolation is used for upsampling in Fig. 7c. The MAE is 0.99 mm, the ISE is 1.51 mm^2, and the peak error is 3.62 mm when EKF based upsampling is used in Fig. 7d. Because, the coefficients of the model (9) used by the EKF can change with time, prediction based on the EKF performed better than using the past heart motion. Also, upsampling based on an EKF performed slightly better than upsampling with cubic interpolation.

B. Approach 2

It is usually difficult to obtain the $_I^R T$ as the position and orientation of the image sensor must be continually tracked in real-time and the $_I^R T$ continually updated, which may become computationally expensive. Also, it may be difficult to track the position and orientation of the image sensor. In this case, the delay must be compensated for within the control loop.

Here, a SP is used to compensate for the delayed distance measurements. Initially, the first SP (Fig. 3) is used where the predicted POI motion is added to the reference signal to counteract the effect of the disturbance (the POI's motion). As only the distance between the robot (surgical tool tip) and the

POI is available, the delayed motion of the POI needs to be calculated. First, the robot-POI distance is upsampled using cubic interpolation and not an EKF, as the EKF requires a quasi-periodic signal. Next, the motion of the robot is measured in real-time in the robot-frame. These measurements are delayed by the length of the data acquisition and processing delay of the sensor and then the robot-POI distance is subtracted. This leaves the POI's delayed position, $^R \bar{P}_O''$. As the distance data was previously upsampled, the POI measurements only need to be predicted. The results are given in Fig. 8. The MAE, ISE, and peak errors are 4.46 mm, 11.3 mm^2, and 24.8 mm respectively when the last heart beat is used to predict the current heart motion shown in Fig. 8a. The MAE, ISE, and peak errors are 4.45 mm, 22.7 mm^2, and 9.39 mm respectively when EKF based prediction is used to predict the current heart motion shown in Fig. 8b. It is clear from Fig. 8b that using an EKF to predict the POI's motion gives a better result than using the POI's previous cycle of motion when the rate of the POI's motion is changing.

Then, the second SP is tested. As the predicted POI's motion is added to the inner feedback loop to account more directly for the disturbance the POI's motion adds to the output (the distance between the surgical tool and the POI), it is expected to give a better result than the previous case. Once again, cubic interpolation must be used to upsample the distance data as was previously discussed. The results are given in Fig. 9. The MAE, ISE, and peak errors are 3.10 mm, 13.3 mm^2, and 8.29 mm respectively when the last heart beat is used to predict the current heart motion shown in Fig. 9a. The MAE, ISE, and peak errors are 1.92 mm, 5.94 mm^2, and 8.36 mm respectively when EKF based prediction is used to predict the current heart motion shown in Fig. 9b. It is clear from Fig. 9b that using an EKF to predict the POI's motion gives a better result than using the previous POI's motion if the rate of the POI's motion is changing. As expected, because the estimated POI motion is subtracted from the robot's position in the inner feedback loop in the same manner as it is subtracted from the robot's actual position in real-time, the second SP configuration performs better than the first.

Finally, as a comparison, a SP can also be used when the $_I^R T$ is available. Here, the current POI motion is estimated directly from the POI motion measurements, $\bar{P}_O'$. As the second SP configuration performed better than the first, only the second configuration was used for this test. The results are given in Fig.10 where cubic interpolation is used, and EKF based prediction is used as it consistently outperformed predicting the current POI motion based on previous motion. The MAE, ISE, and peak error is 1.65 mm, 4.39 mm^2, and 6.28 mm, respectively as shown in Fig.10a.

In all cases, the motion and delay compensation controllers reduced the tracking error significantly as compared to no compensation. Most of the mean tracking errors were reduced to less than 2 mm when the heart moves approximately 10 mm as shown in the summary given in Tab. III. The results consistently show that EKF based prediction and upsampling where possible, performs better than the other methods proving
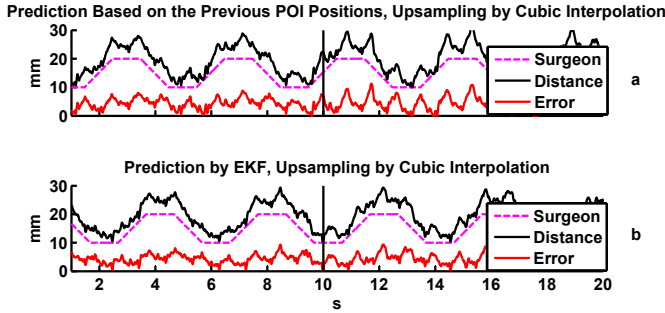
Prediction Based on the Previous POI Positions, Upsampling by Cubic Interpolation

Prediction by EKF, Upsampling by Cubic Interpolation

Fig. 8: The tracking result of using SP method I when the $_I^R T$ is not available. The dashed pink line is the physician's motion, the solid black line is the real-time distance between the surgical tool tip and the POI, and the solid red line is the error between the physician's motion and the real-time distance between the surgical tool tip and the POI. The vertical line denotes the time at which the heart rate increases.
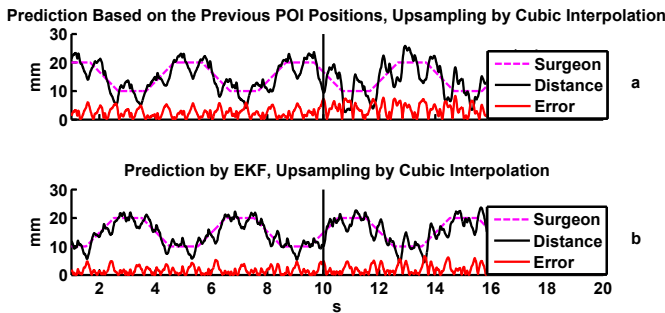

Prediction Based on the Previous POI Positions, Upsampling by Cubic Interpolation

Prediction by EKF, Upsampling by Cubic Interpolation

Fig. 9: The tracking result of using SP method II when the $_I^R T$ is not available. The dashed pink line is the physician's motion, the solid black line is the real-time distance between the surgical tool tip and the POI, and the solid red line is the error between the physician's motion and the real-time distance between the surgical tool tip and the POI. The vertical line denotes the time at which the heart rate increases.

Hypothesis 1. The proportional controller of Fig. 2 performed better than the two SP based controllers. However, this is an unfair comparison as these controllers are used in different situations. If the $_I^R T$ is available, more direct measurements can be taken and, as expected, this case had the best performance. When the $_I^R T$ is not available, the second SP configuration of Fig. 4 outperformed the first of Fig. 3 – proving *Hypothesis 2*. Depending on the availability of the $_I^R T$, both the proportional controller of Fig. 2 and the second SP configuration of Fig. 4 provide satisfactory performance. Both have small position tracking errors, maintain the system's stability despite the image acquisition and processing delay, and can handle a changing rate of the POI's motion.

V. Functional Task

To test the performance of the motion compensating robotic system, a functional task is considered. This task simulates draining fluid from a patient with a pericardial effusion, which is a build-up of fluid within the pericardial sac – see Fig. 11. As the pericardial sac is stiff and does not expand when filled with
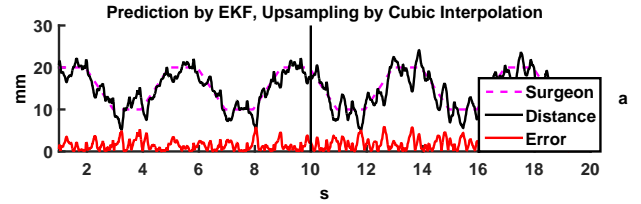

Prediction by EKF, Upsampling by Cubic Interpolation

Fig. 10: The tracking result of using SP method II when the $_I^R T$ is available. The dashed pink line is the surgeon's motion. The solid black line is the real-time distance between the surgical tool tip and the POI. The solid red line is the error between the physician's motion and the real-time distance between the surgical tool tip and the POI.

Controller Type	Upsampling and Prediction	MAE (mm)	ISE (mm^2)	Peak Error (mm)
Proportional	CI and PM	1.23	2.39	4.34
Proportional	EKF and PM	1.07	1.99	5.44
Proportional	CI and EKF	1.14	2.13	4.38
Proportional	EKF and EKF	0.99	1.51	3.62
SP I	CI and PM	4.46	24.8	11.3
SP I	CI and EKF	4.45	22.7	9.39
SP II	CI and PM	3.10	13.3	8.36
SP II	CI and EKF	1.92	5.94	8.36
SP II F	CI and EKF	1.65	4.39	6.28

TABLE III: A summary of the experimental results. Three separate controllers were tested: the control scheme of Fig. 2 (Proportional), and the two SP control schemes of Fig. 3 (SP I) and Fig. 4 (SP II). The final case also uses the SP of Fig. 4 (SP II F), but it is assumed that the $_I^R T$ is available and the POI's motion is measured directly from the images. The two upsampling methods are cubic interpolation (CI) and EKF and the two prediction methods are previous motion (PM) and EKF based.

excess fluid, the excess fluid puts pressure on the heart causing it to beat abnormally. This condition can leave the patient short of breath. To drain the excess fluid and relieve the pressure, a needle is inserted through the patient's chest wall and into the pericardial sac. A guide wire is then inserted through the needle, the needle is withdrawn, and a drainage tube is inserted over the guide wire. The difficulty in performing this procedure is to puncture the pericardial sac without puncturing a coronary artery, as this would require immediate surgery.
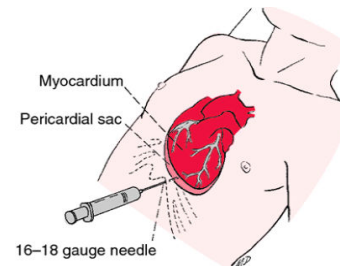

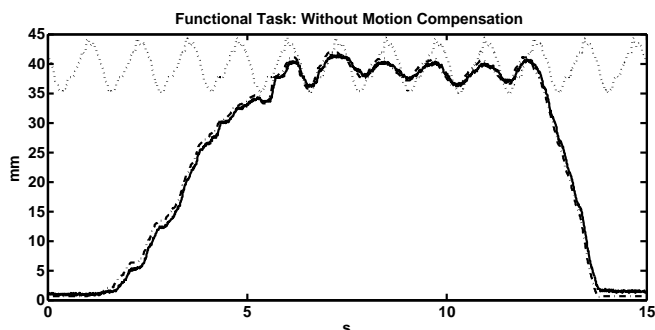Fig. 11: A diagram showing how pericardiocentesis is performed [31].

Fig. 12: The tracking result of the functional task when motion compensation is not provided. Here, the dotted line is the POI's motion, the solid line is the robot's motion, and the dash-dotted line is the surgeon's motion. The shapes of the two curves do not match. It is very difficult for the surgeon to control the back and forth motion of the robot from the user interface quickly enough to match the POI's motion while also performing the surgical task.
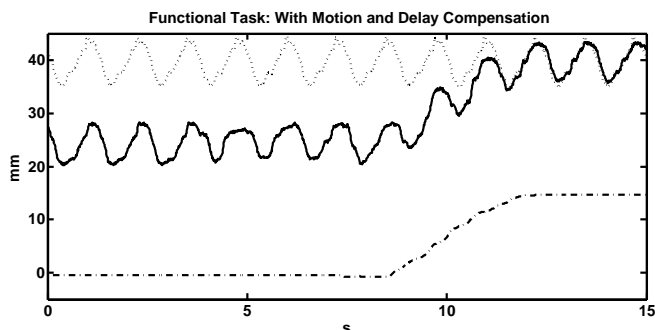

Fig. 13: The tracking result of the functional task when motion compensation is provided. Here, the dotted line is the POI's motion, the solid line is the robot's motion, and the dash-dotted line is the surgeon's motion. The shapes of the two motion curves are similar except for the surgeon's purposeful motions that move the robot close to the heart to withdraw fluid at 9 s.

To simulate this functional task, a small cylindrical container is placed within a larger one. The smaller container is filled with coloured water (simulating blood in an artery) and is covered by a latex membrane. The larger container is filled with clear water (simulating the excess fluid to be drained from the pericardial sac) and is also covered by a latex membrane. There is a 5 mm gap between the two membranes. This set of two containers is mounted on the mechanical cam and moves in a similar manner as a point on the heart surface. The goal of this task is to puncture the outer membrane with a needle that is attached to a teleoperated robot and withdraw 1 ml of clear fluid. Since the inner membrane represents the coronary artery, if it is punctured the coloured fluid will be withdrawn and the test will be considered a failure.

Three tests to extract the fluid are performed. In the first case, there is no motion compensation; rather, the robot follows the surgeon's motions. The result is shown in Fig. 12, where the dotted line, the dash-dotted line, and the solid line are the POI's, surgeon's and robot's motion, respectively.
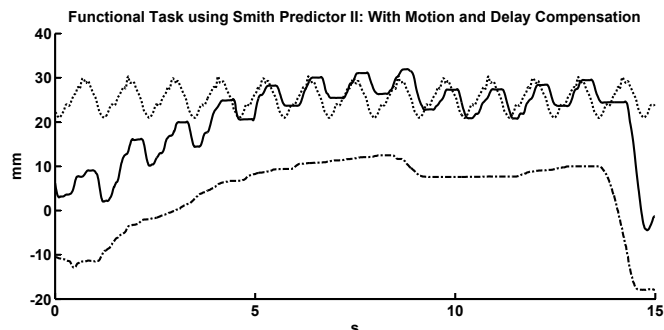

Fig. 14: The tracking result of the functional task when motion compensation is provided by the second SP. Here, the dotted line is the POI's motion, the solid line is the robot's motion, and the dash-dotted line is the surgeon's motion. The shapes of the two motion curves are similar except for the surgeon's purposeful motions that move the robot close to the heart to withdraw fluid.

As the surgeon must manually compensate for the heart's motion while extracting the fluid, the tracking of the heart's motion is poor and the coloured fluid is extracted meaning the needle would have punctured the heart if this were an actual procedure. In the second case, robotic motion compensation is provided using the control scheme of Fig. 2. The result is shown in Fig. 13, where the dotted line is the POI's motion, the dash-dotted line is the surgeon's motion and the solid line is the robot's motion. Here, the surgeon only needs to move the robot towards the POI to set the desired position for the extracting the fluid. The robot follows both the surgeon's and the POI's motion. The tracking result is significantly better in this case and only the clear fluid is extracted. Finally, SP method II is tested. The results are shown in Fig 14, where the dotted line is the POI's motion, the dash-dotted line is the surgeon's motion and the solid line is the robot's motion. Once again, the surgeon only needs to move the robot towards the POI to set the desired position for the extracting the fluid. The robot follows both the surgeon's and the POI's motion and only the clear fluid is extracted.

VI. DISCUSSION

The results presented in this work are for a more challenging case compared to the previous literature. In this work, the POI motion data was first upsampled and predicted ahead to compensate for the image acquisition and processing delays. These delays were approximately 180 ms. The errors reported for POI motion of 10 mm have average values of approximately 0.99 mm to 1.59 mm and peak values of approximately 3.62 mm to 5.90 mm for the best cases when a proportional controller and a SP method II were used. Some of the literature have reported smaller errors, but these cases did not all include upsampling or motion compensation for such large image acquisition and processing delays.

Using pre-recorded position data from sonomicrometry crystals sutured to the heart, average errors as low as 0.669 mm were reported in [16], but the peak errors were as large as

4.3 mm. This method is not clinically viable as it is not real-time and the crystals must be sutured onto the POI site.

In [9] the residual motion (approximately 6 and 8 mm in the x and y directions) left after mechanically stabilizing the heart was compensated for by moving a 40 Hz endoscope to stabilize the image. However, this method does not let the heart beat freely and is only viable on the exterior heart surface. Mean errors of approximately 0.4 and 0.8 mm in the x and y directions and a peak error of approximately 2 mm in the y-direction were reported.

In [19] position data was collected from a 500 Hz camera. A one sample ahead predictive controller was able to reduce the tracking error to less than a millimetre. However, in this case, the position data is collected at a very fast rate meaning there is less movement between samples and the length of the prediction is much shorter.

In the most similar case to this work, Yuen et al. reported an average and peak error of 0.97 mm and 3.26 mm respectively on simulated heart motion data with a peak-to-peak amplitude of 12.36 mm [20]. These errors are very similar to those reported in this work; however, Yuen et al. used a sampling rate of 28 Hz and therefore only predicted one time step ahead.

Future work will include the extension of this work for multi-dimensional motion compensation. This method could also benefit from the addition of ECG data that will provide information about the upcoming position of the POI.

VII. Conclusion

Surgical or therapeutic procedures are difficult for physicians to perform if the POI is continually moving due to physiological motion caused by respiration or the beating heart. To aid the physician, a robot-assisted system is designed to compensate for the POI's physiological motion. The difficulty in creating such a system is that the position measurements of the POI are slowly sampled, delayed, and possibly not registered to the robot's frame of reference. Three controllers are presented in this work that overcome these challenges. The first assumes the $^R_I T$ is available such that the POI's position measurements can be transformed into the robot frame. In this case, the POI's position measurements are upsampled and predicted ahead to overcome the delay. Now, a regular controller can be used to ensure that the distance between the robot and the POI follows the physician's motion. When the $^R_I T$ is not available, the distance between the POI and the robot is measured. In this case the POI's motion is calculated from the robot's position and the upsampled distance measurements. In the second approach, a SP, which compensates for the delay, is used in the feedback control loop. Two different configurations are proposed; the first adds the predicted POI motion to the surgeon's to form a new setpoint, and the seconds adds the predicted POI motion into the inner feedback loop to reflect where the POI's actual motion is added into the system. As expected, the second method which adds the predicted POI motion to the inner feedback loop performs better than the first.
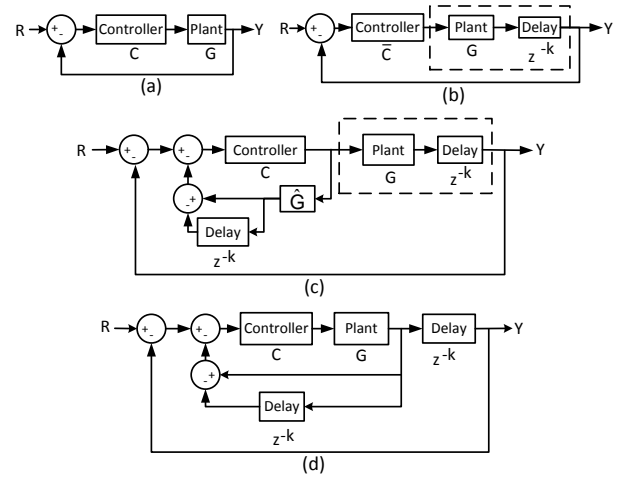

Fig. 15: (a): A standard plant and feedback controller without a time delay. (b): A standard plant and feedback controller with time delay. (c): A SP, where the plant's model must be estimated. (d): A SP, where the plant's model does not need to be estimated.

Appendix

A SP is a predictive feedback controller that, in the presence of a known and fixed time delay, ensures the stability and good performance of a closed-loop control system [30]. Consider the feedback loops in Figs. 15a and b. To begin, the controller C is designed for closed-loop feedback system without a delay, see Fig. 15a, where the transfer function is given by H.

$$H = \frac{Y}{R} = \frac{CG}{1 + CG}. \tag{17}$$

where G is the plant transfer function, R and Y are the Laplace transforms of the plant's input and output, respectively.

In Fig. 15b, the plant G is replaced by a plant with a fixed time delay k, Gz^{-k}. Here, the controller C is replaced with $\bar{C}$ and the closed-loop transfer function becomes $\bar{H}$.

$$\bar{H} = \frac{Y}{R} = \frac{\bar{C}Gz^{-k}}{1 + \bar{C}Gz^{-k}}. \tag{18}$$

To retain the same performance as the system that without a time delay, the transfer function of the delayed system should equal that of the system without a delay multiplied by the time delay, i.e., $\bar{H} = Hz^{-k}$. $\bar{C}$ is calculated from this equality.

$$\bar{C} = \frac{C}{1 + CG(1 - z^{-k})}. \tag{19}$$

The SP $\bar{C}$ in Fig. 15c requires an estimate of the plant, $\hat{G}$. However, if the plant can be separated from the delay, we do not need the estimate of the plant's model; rather, the output of the plant can be used directly – see Fig. 15d.

References

[1] A. Bó, P. Poignet, and C. Geny, "Pathological tremor and voluntary motion modeling and online estimation for active compensation," *IEEE Trans. on Neural Systems and Rehabilitation Engineering*, vol. 19, no. 2, pp. 177–185, April 2011.

[2] H. Shirato, S. Shimizu, T. Kunieda, K. Kitamura, M. van Herk, K. Kagei, T. Nishioka, S. Hashimoto, K. Fujita, H. Aoyama, K. Tsuchiya, K. Kudo, and K. Miyasaka, "Physical aspects of a real-time tumor-tracking system for gated radiotherapy," *Int. Journal of Radiation Oncology Biology Physics*, vol. 48, no. 4, pp. 1187–1195, 2000.

[3] A. Bel, O. Petrascu, I. Van de Vondel, L. Coppens, N. Linthout, D. Verellen, and G. Storme, "A computerized remote table control for fast on-line patient repositioning: Implementation and clinical feasibility," *Medical Physics*, vol. 27, no. 2, pp. 354–358, 2000.

[4] P. J. Keall, V. R. Kini, S. S. Vedam, and R. Mohan, "Motion adaptive X-ray therapy: a feasibility study," *Physics in Medicine and Biology*, vol. 46, no. 1, pp. 1–10, 2001.

[5] T. Neicu, H. Shirato, Y. Seppenwoolde, and S. B. Jiang, "Synchronized moving aperture radiation therapy (SMART): average tumour trajectory for lung patients," *Physics in Medicine and Biology*, vol. 48, no. 5, pp. 587–598, 2003.

[6] M. J. Murphy, "Tracking moving organs in real time," *Seminars in Radiation Oncology*, vol. 14, no. 1, pp. 91–100, 2004.

[7] J. R. Adler, S. D. Chang, M. J. Murphy, J. Doty, P. Geis, and S. L. Hancock, "The Cyberknife: A frameless robotic system for radiosurgery," *Stereotactic and Functional Neurosurgery*, vol. 69, pp. 124–128, 1997.

[8] D. Fu, R. Kahn, B. Wang, H. Wang, Z. Mu, J. Park, G. Kuduvalli, and C. Maurer, "Xsight lung tracking system: A fiducial-less method for respiratory motion tracking," in *Treating Tumors that Move with Respiration*, H. Urschel, J. Kresl, J. Luketich, L. Papiez, R. Timmerman, and R. Schulz, Eds. Springer Berlin Heidelberg, 2007, pp. 265–282.

[9] T. Ortmaier, M. Gröger, D. H. Boehm, V. Falk, and G. Hirzinger, "Motion estimation in beating heart surgery," *IEEE Trans. on Biomedical Engineering*, vol. 52, no. 10, pp. 1729–1740, 2005.

[10] M. F. Newman, J. L. Kirchner, B. Phillips-Bute, V. Gaver, H. Grocott, R. H. Jones, D. B. Mark, J. G. Reves, and J. A. Blumenthal, "Longitudinal assessment of neurocognitive function after coronary-artery bypass surgery," *New England Journal of Medicine*, vol. 344, no. 6, pp. 395–402, 02/08 2001.

[11] G. Reed, D. Singer, E. Picard, and R. DeSanctis, "Stroke following coronary-artery bypass surgery. A case-control estimate of the risk from carotid bruits," *The New England Journal of Medicine*, vol. 319, pp. 1246–1250, 1988.

[12] Y. Nakamura, K. Kishi, and H. Kawakami, "Heartbeat synchronization for robotic cardiac surgery," in *IEEE Int. Conf. on Robotics and Automation*, vol. 2, 2001, pp. 2014–2019.

[13] M. Dominici and R. Cortesao, "Model predictive control architectures with force feedback for robotic-assisted beating heart surgery," in *IEEE Int. Conf. on Robotics and Automation*, 2014, pp. 2276–2282.

[14] S. Kesner and R. Howe, "Motion compensated catheter ablation of the beating heart using image guidance and force control," in *Int. Symposium on Experimental Robotics*, 2012, pp. 579–590.

[15] O. Bebek and M. Çavuşoğlu, "Whisker-like position sensor for measuring physiological motion," *IEEE/ASME Trans. on Mechatronics*, vol. 13, no. 5, pp. 538–547, Oct 2008.

[16] O. Bebek and M. C. Çavuşoğlu, "Intelligent control algorithms for robotic-assisted beating heart surgery," *IEEE Trans. on Robotics*, vol. 23, no. 3, pp. 468–480, 2007.

[17] E. E. Tuna, J. H. Karimov, T. Liu, O. Bebek, K. Fukamachi, and M. C. Cavusoglu, "Towards active tracking of beating heart motion in the presence of arrhythmia for robotic assisted beating heart surgery," *PLoS ONE*, vol. 9, no. 7, p. e102877, 07 2014.

[18] T. J. Franke, O. Bebek, and M. C. Çavuşoğlu, "Improved prediction of heart motion using an adaptive filter for robot assisted beating heart surgery," in *IEEE/RSJ Int. Conf. on Intelligent Robots and Systems*, 2007, pp. 509–515.

[19] R. Ginhoux, J. Gangloff, M. de Mathelin, L. Soler, M. M. A. Sanchez, and J. Marescaux, "Active filtering of physiological motion in robotized surgery using predictive control," *IEEE Trans. on Robotics*, vol. 21, no. 1, pp. 67–79, 2005.

[20] S. G. Yuen, P. M. Novotny, and R. D. Howe, "Quasiperiodic predictive filtering for robot-assisted beating heart surgery," in *IEEE Int. Conf. on Robotics and Automation*, 2008, pp. 3875–3880.

[21] M. Bowthorpe, M. Tavakoli, H. Becher, and R. Howe, "Smith predictor based robot control in ultrasound-guided teleoperated beating-heart surgery," *IEEE Journal of Biomedical and Health Informatics*, vol. 18, no. 1, pp. 157–166, 2013.

[22] J. Schwaab, M. Prall, C. Sarti, R. Kaderka, C. Bert, C. Kurz, K. Parodi, M. Günther, and J. Jenne, "Ultrasound tracking for intra-fractional motion compensation in radiation therapy," *Physica Medica*, vol. 30, no. 5, pp. 578–582, 2014, particle Radiosurgery Conference.

[23] M. F. Kruis, J. B. van de Kamer, A. C. Houweling, J.-J. Sonke, J. S. Belderbos, and M. van Herk, "PET motion compensation for radiation therapy using a CT-based mid-position motion model: Methodology and clinical evaluation," *International Journal of Radiation Oncology Biology Physics*, vol. 87, no. 2, pp. 394–400, 2013.

[24] S. Xu, G. Fichtinger, R. H. Taylor, and K. R. Cleary, "3D motion tracking of pulmonary lesions using ct fluoroscopy images for robotically assisted lung biopsy," *Proc. SPIE*, vol. 5367, pp. 394–402, 2004.

[25] W.-K. Wong, B. Yang, C. Liu, and P. Poignet, "A quasi-spherical triangle-based approach for efficient 3-d soft-tissue motion tracking," *IEEE/ASME Trans. on Mechatronics*, vol. 18, no. 5, pp. 1472–1484, Oct 2013.

[26] D. T. Kettler, R. D. Plowes, P. M. Novotny, N. V. Vasilyev, P. J. del Nido, and R. D. Howe, "An active motion compensation instrument for beating heart mitral valve surgery," in *IEEE/RSJ Int. Conf. on Intelligent Robots and Systems*, 2007, pp. 1290–1295.

[27] A. Zahraee, J. Paik, J. Szewczyk, and G. Morel, "Toward the development of a hand-held surgical robot for laparoscopy," *IEEE/ASME Trans. on Mechatronics*, vol. 15, no. 6, pp. 853–861, Dec 2010.

[28] J. Rotella, "Predictive tracking of quasi periodic signals for active relative motion cancellation in robotic assisted coronary artery bypass graft surgery," Master's thesis, Case Western Reserve University, 2005.

[29] P. J. Parker and B. D. Anderson, "Frequency tracking of nonsinusoidal periodic signals in noise," *Signal Processing*, vol. 20, no. 2, pp. 127–152, 1990.

[30] O. J. M. Smith, "Closer control of loops with dead time," *Chemical Engineering Progress*, vol. 53, pp. 217–219, 1957.

[31] *Miller-Keane Encyclopedia and Dictionary of Medicine, Nursing, and Allied Health, Seventh Edition*. Saunders, 2003.
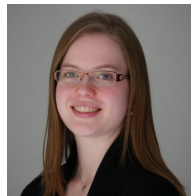
Meaghan Bowthorpe received her B.Sc. degree in Electrical Engineering from the University of Alberta in 2010. She is currently pursuing a Ph.D. in Electrical and Computer Engineering at the University of Alberta and is working on motion tracking algorithms for image-guided robot-assisted surgery.

Mahdi Tavakoli is an Associate Professor in the Department of Electrical and Computer Engineering, University of Alberta, Canada. He received his BSc and MSc degrees in Electrical Engineering from Ferdowsi University and K.N. Toosi University, Iran, in 1996 and 1999, respectively. He received his PhD degree in Electrical and Computer Engineering from the University of Western Ontario, Canada, in 2005. In 2006, he was a post-doctoral researcher at Canadian Surgical Technologies and Advanced Robotics (CSTAR), Canada. In 2007-2008, he was an NSERC Post-Doctoral Fellow at Harvard University, USA. Dr. Tavakoli's research interests broadly involve the areas of robotics and systems control. Specifically, his research focuses on haptics and teleoperation control, medical robotics, and image-guided surgery. Dr. Tavakoli is the lead author of Haptics for Teleoperated Surgical Robotic Systems (World Scientific, 2008).